Climate Dynamics (1999) 15:737–750

S. Yang · K.-M. Lau · P. S. Schopf

Sensitivity of the tropical Pacific Ocean to precipitation-induced freshwater flux

Received: 10 July 1998 / Accepted: 2 February 1999

Abstract We have performed experiments using an ocean model to study the sensitivity of tropical Pacific Ocean to variations in precipitation induced freshwater fluxes. Variations in these fluxes arise from natural causes on all time scales. In addition, estimates of these fluxes are uncertain because of differences among measurement techniques. The model used is a quasi-isopycnal model, covering the Pacific from 40 °S to 40 °N. The surface forcing is constructed from observed wind stress, evaporation, precipitation, and sea surface temperature (SST) fields. The heat flux is produced with an iterative technique so as to maintain the model close to the observed climatology, but with only a weak damping to that climatology. Climatological estimates of evaporation are combined with various estimates of precipitation to determine the net surface freshwater flux. Results indicate that increased freshwater input decreases salinity as expected, but increases temperatures in the upper ocean. Using the freshwater flux estimated from the Microwave Sounding Unit leads to a warming of up to 0.6 °C in the western Pacific over a case with zero net freshwater flux. SST is sensitive to the discrepancies among different precipitation observations, with root-mean-square differences in SST on the order of 0.2–0.3 °C. The change in SST is more pronounced in the eastern Pacific, with difference of over 1 °C found among the various precipitation products. Interannual variation in precipitation during El Niño events leads to increased warming. During the winter of 1982–83, freshwater flux accounts for about 0.4 °C (approximately 10–15% of the maximum warming) of the surface warming in the central-eastern Pacific. Thus, the error of SST caused by the discrepancies in precipitation products is more than half of the SST anomaly produced by the interannual variability of observed precipitation. Further experiments, in which freshwater flux anomalies are imposed in the western, central, and eastern Pacific, show that the influence of net freshwater flux is also spatially dependent. The imposition of freshwater flux in the far western Pacific leads to a trapping of salinity anomalies to the surface layers near the equator. An identical flux imposed in the central Pacific produces deeper and off-equatorial salinity anomalies. The contrast between these two simulations is consistent with other simulations of the western Pacific barrier layer formation.

S. Yang[1](✉) · K.-M. Lau
Laboratory for Atmospheres, Climate and Radiation Branch, NASA-Goddard Space Flight Center, Greenbelt, MD, USA
e-mail: yang@climate.gsfc.nasa.gov

Also at:
[1] SAIC/General Sciences Corporation, Beltsville, MD, USA

P. S. Schopf
Institute of Computational Sciences and Informatics, George Mason University, Fairfax, Virginia, USA

1 Introduction

Although the importance of freshwater flux for understanding the extratropical ocean was noticed more than a century ago (Hough 1897), its effect on tropical ocean dynamics has not received attention until recent years. The dearth in scientific research in this area is due not only to the difficulties in obtaining reliable observations such as salinity and precipitation over oceans but also to the commonly accepted notion that for tropical upper oceans freshwater flux is of secondary importance to wind stress. Indeed, without considering the contribution from salinity, some observational and modeling studies are reasonably successful in explaining many basic features of the major currents of world's oceans (Gill 1982). However, recent studies that consider the effect of salinity have revealed important features of ocean structure that are absent from many previous works in which salinity effect is excluded.

During the past two decades, many ocean observational data have become available because of the advent of satellites and many internationally collaborative programs. The accumulated observations have provided better tools for understanding the role of freshwater flux in upper ocean dynamics (Price 1979; Lukas and Lindstrom 1991; You 1995; Anso and McPhaden 1997; Li et al. 1998). In particular, studies using data from the Tropical Ocean Global Atmosphere Coupled Ocean-Atmosphere Response Experiment (Webster and Lukas 1992) have indicated a close relationship between precipitation and salinity on various time scales. The discovery of the barrier layer (Godfrey and Lindstrom 1989; Lukas and Lindstrom 1991) has improved our understanding of the upper ocean dynamics of the western tropical Pacific. In addition, it has been shown that under certain circumstances freshwater flux can be as important as net surface heat flux in determining surface buoyancy flux (e.g. Weller and Anderson 1995; Cronin and McPhaden 1998).

Both ocean mixed layer models (e.g., Miller 1976; Anderson et al. 1996; Li et al. 1998) and general circulation models (GCMs; Copper 1988; Carton 1991; Reason 1992; Huang 1993; Murtugudde and Busalacch 1998) have been used to investigate the role of freshwater flux in upper ocean dynamics. Studies using mixed layer models have revealed that precipitation alters significantly the structure of ocean surface layer including density stratification and the depth of the surface layer. The more complex GCMs have also shown that freshwater flux causes changes in ocean salinity, current, and temperature fields. In particular, Murtugudde and Busalacchi (1998) showed that freshwater input could lead to an increase in sea surface temperature (SST) by as much as 0.5 °C. They suggested that the effect of salinity should not be neglected in operational models for realistic forecasts of tropical oceans. The GCM experiments by Reason (1992) showed that the ocean response to the El Niño and La Niña type precipitation anomalies is apparently different.

Because freshwater flux (precipitation minus evaportation; $P - E$) is a part of the fully coupled system, it is difficult for observational studies to isolate the influence of freshwater on ocean response from the impact of other factors such as wind stress and heat flux. This suggests the importance of ocean modeling. However, model results depend on the models used. They are also sensitive to experiment design including the methods dealing with boundary conditions. For example, Carton (1991) showed that freshwater flux changed the SST of tropical Atlantic Ocean by only about 0.1 °C. On the other hand, Murtugudde and Busalacchi (1998) found a much larger impact of freshwater flux on SST. The two studies used different models and treated the boundary conditions for temperature in different ways. Thus, the discrepancy between the two studies may due either to the models used or to the treatment for boundary conditions, or to both.

Another source of error in evaluating the impact of freshwater fluxes on ocean dynamic is the uncertainties in these fluxes. Currently, there are many precipitation products that can be used in ocean model experiments. More satellite-gage combined precipitation estimates emerge with the recent launch of Tropical Rainfall Measuring Mission. However, substantial discrepancies exist among the various products (e.g., Lau et al. 1996; see also Fig. 1 later) and these discrepancies cause inconvenience for both research and operational practice. We need to recognize the level of observational error that we can tolerate. One way to evaluate the "error tolerance" level of these products is to examine their impacts on ocean model performance.

The objectives of this study are twofold: (1) to explore the sensitivity of upper Pacific response to different precipitation forcings and (2) to unravel basic oceanic processes that are responsible for such sensitivity. To facilitate the assessment of the significance of ocean response to the discrepancies in precipitation observations, we will first estimate the impact of total $P - E$ on the ocean. We will then carry out a series of sensitivity and anomaly experiments and systematically investigate the consequences of freshwater forcings.

The outline is as follows. In Sect. 2, we describe the model, forcing fields, and experimental design. In Sect. 3, we compare the simulated temperature and salinity with observations. The sensitivity of ocean response to different precipitation products is shown in Sect. 4. In Sect. 5, we address the response of upper ocean to El Niño and La Niña related precipitation anomalies and compare this response with that discussed in Sect. 4. To provide further support for the discussion in Sect. 4 and Sect. 5, we examine results from additional experiments in Sect. 6. Finally, we summarize the results in Sect. 7.

2 Methodology

2.1 Model

The model used in this study is a quasi-isopycnal general circulation model as described in Schopf and Loughe (1995). It is an "operational" ocean model used in the NASA Seasonal-to-Interannual Prediction Project. The model is coded in latitude-longitude orthogonal curvilinear coordinates with a generalized vertical coordinate. The horizontal resolution is (2/3)° latitude by 1.25° longitude. In the vertical, for which a hydrostatic Boussinesq approximation is applied, 14 active layers overlie a quiescent deep ocean. The number of layers has been increased from Schopf and Loughe (1995) to better resolve the thermocline structure. Each of the upper 10 layers is allowed to become no thinner than 10 m, at which point the quasi-isopycnal treatment will cause cross-coordinate mass, heat, salt, and momentum fluxes to be invoked for conservation. This limit is thinner than that employed by Schopf and Loughe (1995) reflecting the increase in the number of layers.

The model is designed to handle internal shear-induced mixing, convective overturning, and the surface turbulent mixing generated by wind stirring and surface cooling in the topmost model layer. The

surface layer is treated as a bulk turbulent well-mixed layer in a way similar to Niiler and Kraus (1977). It is incorporated in the model through the prescription of a cross-coordinate mass flux at the base of the layer. The flux is computed through a balance between wind stirring, release of mean kinetic energy, dissipation, and the increase in potential energy because of mixing. Mass flux across the surface of the ocean is determined by the values of precipitation and evaporation. For the model's subsurface layers, the vertical mixing scheme of Pacanowski and Philander (1981) is used, with a background diffusivity of 10^{-5} m^2 s^{-1} for temperature and 10^{-4} m^2 s^{-1} for salt. In the horizontal, an 8th order Shapiro (1970) filter is applied to momentum and layer thickness, and a 4th order filter to temperature and salinity. These filters are employed once per day for all these fields. For a more detailed description of the model, readers are referred to Schopf and Loughe (1995) and Yu and Schopf (1977).

In this study, the model domain covers the Pacific basin of 40 °S–40 °N, 120 °E–80 °W. Realistic coastlines are placed at the western and eastern boundaries. The northern and southern boundaries are treated as artifical walls, though which mass fluxes are zero. There are no sponge layers at the northern and southern walls that prevent reflection of energy back into the model domain. Among the 14 vertical layers, at least 8 layers are within the top 300 m in the equatorial region.

2.2 Surface forcing fields

The surface forcing fields used in this study include wind stress, heat flux, precipitation, and evaporation. Precipitation data are from the data sets of Microwave Sounding Unit (MSU; Spencer 1993), Global Precipitation Climatology Project (GPCP; Huffman et al. 1997), Pathfinder (George Huffmann 1997, personal communication), Jaeger (1976), and CPC Merged Analysis of Precipitation (CMAP; Xie and Arkin 1996). While the MSU is a microwave only estimate, the CMAP data combines both IR and microwave information. Jaeger precipitation is based on in-situ observation and available only as climatology. Figure 1 shows the annual climatologies and the root-mean-square (rms) errors of these five precipitation products. The figure indicates that the largest discrepancies among these products are in the magnitude of the intertropical convergence zone (ITCZ) over the central and eastern Pacific. Over the western Pacific warm pool, most precipitation appears in CMAP and least in MSU. Overall, there is a large similarity between the GPCP and Pathfinder patterns. Figure 1f delineates three significant centers of rms error over 2 °N/170 °E, 10 °S/175 °E, and 6 °N/135 °W, respectively. Over the central-eastern equatorial Pacific (e.g., 0 °N/120 °W), the errors can be larger than 50% of the total precipitation. As indicated in the introduction, the sensitivity of upper ocean response to the discrepancies among these precipitation observations is one of the focuses of this study.

This study uses surface evaporation data from the Comprehensive Ocean-Atmosphere Data Set (COADS). Wind stress data are from the Hellerman and Rosenstein (HR; 1983) and Florida State University (FSU) datasets. As in Yu et al. (1997), the magnitude of the HR wind is reduced by 20%. The treatment for surface heat flux will be discussed in the next subsection.

2.3 Experiments

We first carry out a spin-up run to provide initial conditions and some surface forcing fields for all experiments analyzed in this study. In this spin-up run, the model is initialized from Levitus' temperature and salinity (Levitus 1982) and a geostrophic approximation for currents. It is then run for 10 y, forced by the monthly climatologies of HR wind stress, MSU precipitation, and COADS evaporation. The boundary conditions for temperature and salinity are defined in different ways. While the changes of salinity are determined by explicit $P - E$ flux, the net surface heat flux (Qo) is computed as a strong damping to the observed SST (Reynolds and Smith 1994). Following the technique of Haney (1971), we specify the net surface heat flux as $Q\text{o} = K\,(T_{obs}\text{–}T)$, in which K is 100 W m^{-2} K^{-1}.

The net surface heat flux from the spin-up run can be used as the heat flux that would keep the model SST near the observed, given identical inputs of momentum and salinity. As noted in Schopf (1985), the use of such a strong damping to the observed SST is unrealistic, since the surface air temperature is so closely coupled to the SST. Any perturbation run with such a boundary condition on SST would overly damp the SST response. To overcome this problem, Schopf and Loughe (1995) describe a technique where the surface heat flux is replaced by that computed during the spin-up run plus a very weak damping back to the observations. In all the subsequent experiments, the surface heat fluxes from the average of the last two years of the spin-up run are used for the surface forcing, together with a damping coefficient of 10 W m^{-2} K^{-1}. This value was found to provide a good simulation of El Niño variability in Schopf and Loughe (1995). For salinity, the evaporation field is retained from the spin-up run, while different estimates of the precipitation are used to complete the calculation of net freshwater flux. The model utilizes an open upper boundary condition, in which freshwater is explicitly added to the ocean. While the addition of water to the ocean implies the addition of heat, we have assumed that the precipitation and evaporation involve a mass flux at the temperature of sea surface. In this way, changes in SST are due to the dynamical response of the ocean.

Unless specified, only the output from the last year's integration of each experiment is discussed.

2.3.1 *Experiments SO, S1, S2, S3, S4, and S5*

To assess the sensitivity of upper ocean response to different precipitation observations, we carry out five experiments (S1, S2, S3, S4, and S5; S stands for sensitivity) using the precipitation products shown in Fig. 1. Table 1 summarizes the main features of the design for these experiments, in which the climatological annual cycle of surface forcing fields is used. In each experiment, the model was run for 10 y, forced by the HR wind stress. To assess the role of the $P - E$ forcing and to better estimate the relative significance of ocean response to the different precipitation products, we carry out an additional parallel experiment (S0), in which the net freshwater flux is set to zero for all grid points of the entire domain. The results from these experiments will be discussed in Sect. 4.

2.3.2 *Experiments A1 and A2*

We perform two other experiments, A1 and A2 (A stands for anomaly), to evaluate the sensitivity of oceanic response to El Niño/Southern Oscillations (ENSO) related precipitation anomalies and to compare it with the sensitivity to the uncertainties in precipitation inputs seen from experiments S1–S5. As shown in Table 2 that lists the main features of experiment design, both experiments use the monthly mean FSU wind stress. However, while monthly observed MSU precipitation is used in experiment A1, only the climatological annual cycle of the product is applied in A2. The results from these two experiments will be discussed in Sect. 5.

3 Model-observation comparison

Previous studies have shown that the model used in this study can simulate reasonably well many basic features of the upper tropical oceans. Here, we only compare the model result with observations for the

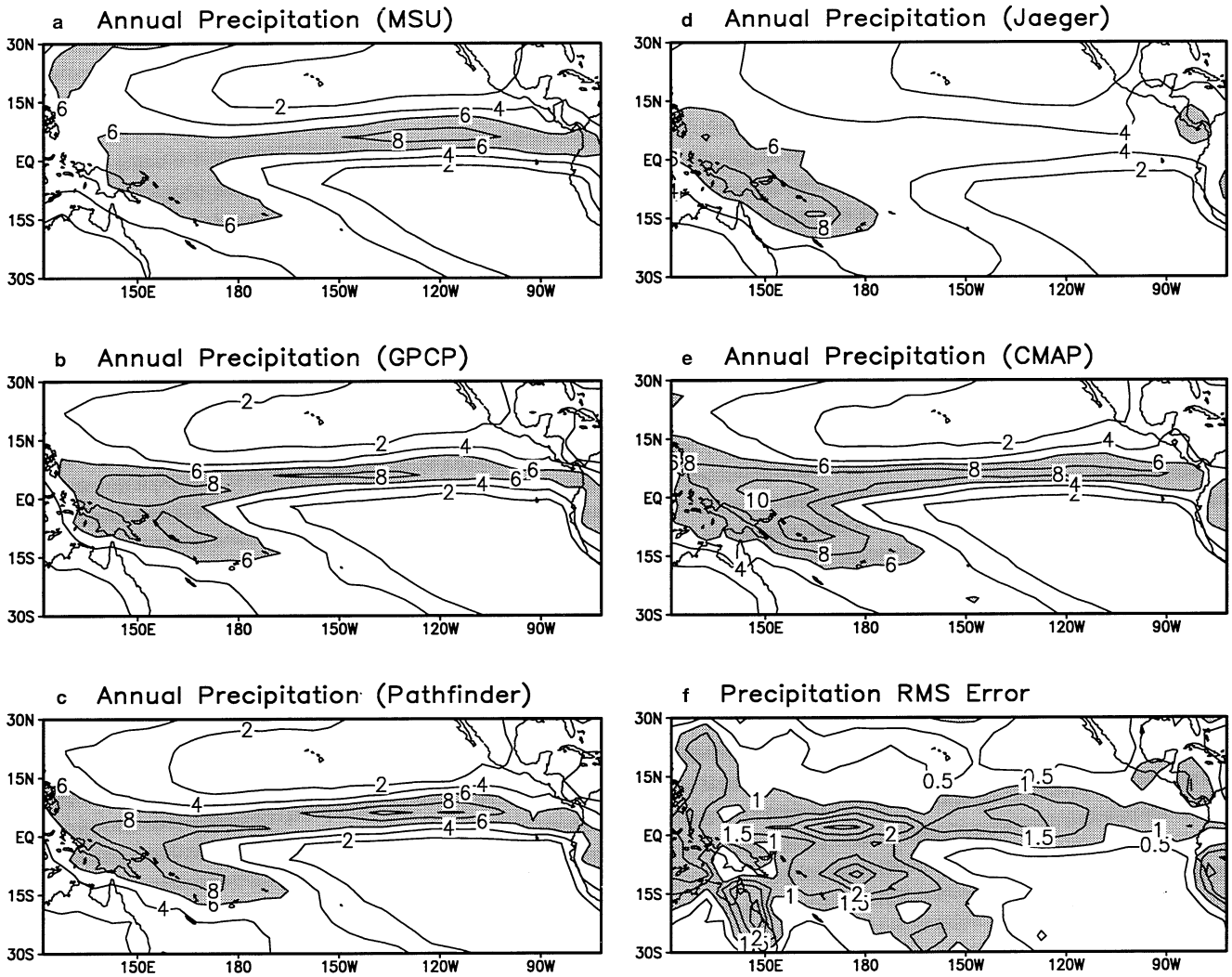

Fig. 1a–f Annual climatological patterns of precipitation from **a** MSU, **b** GPCP, **c** Pathfinder, **d** Jaeger, and **e** CMAP. **f** shows the root-mean-square errors among these precipitation products. Units: mm per day

temperature and salinity fields. For more information about the performance of the model, readers should refer to Schopf and Loughe (1995) and Yu et al. (1997).

Figure 2 shows the patterns of observed SST and temperature at 100 m ($T100$) and those from the 10th year's output from experiment S1. The differences in temperature between observation and simulation are also shown in the figure. Experiment S1 is analyzed here because it uses MSU data set, which is a primary precipitation product used in this study. The observed and simulated fields are quite similar. For example, the model captures the main features of the observed SST reasonably well (Fig. 2a–c). The magnitude of western Pacific warm pool is comparable between observation and model result. Figure 2c shows that the model overestimates slightly the SST under the Pacific ITCZ and underestimates that of the cold tongue in the eastern equatorial Pacific. Because of the nature of the damping flux used in this study, the discrepancy between the simulated and observed SST will look like the pattern of net surface heat flux. Thus, the cold tongue simulated is colder than the observed because the ocean receives heat from the atmosphere and the ocean under the ITCZ is warmer than observations because it gives up heat to the atmosphere. A technique for tackling this problem is discussed in Schopf and Loughe (1995), but the additional effort does not bring substantial benefit to the comparison studies done here.

It is interesting to note that the simulated $T100$ also mimics the observed field (Fig. 2d–f). The model warm pool of western Pacific measured by $T100$ appears reasonably well. In the western subtropical Pacific (about 15 °N), a secondary maximum center appears in both observed and simulated fields. Again, as seen from the SST patterns, the model performs better in

Table 1 Main features of sensitivity experiments

Experiment	Wind stress	Precipitation forcing	Years
S0	HR	$P - E$ set to zero at every grid point	10
S1	HR	MSU; climatological annual cycle	10
S2	HR	GPCP; climatological annual cycle	10
S3	HR	Pathfinder; climatological annual cycle	10
S4	HR	CMAP; climatological annual cycle	10
S5	HR	Jaeger; climatological annual cycle	10

Table 2 Main features of precipitation anomaly experiments

Experiment	Wind stress	Precipitation forcing	Years
A1	FSU; monthly mean observations	MSU; monthly mean observations	10
A2	FSU; monthly mean observation	MSU; climatological annual cycle	10

simulating the warm pool than in capturing the feature of the cool tongue to the east.

Figure 3 shows the patterns of sea surface salinity (SSS) from the Levitus (1982) dataset and experiment S1. The model generally captures the main features of the observed SSS. In both panels, a high SSS enter appears in the Southern Hemisphere with a maximum near 20 °S. There is a narrow band of high SSS in the northern subtropical Pacific. Relatively fresher water exists in the northern tropics, especially in the western and eastern Pacific. An obvious observation-simulation discrepancy occurs in tropical northwestern Pacific. A fresh tongue appears from the model but not the observation. The factors that contribute to this discrepancy may include the possible inadequacies in model physics, the uncertainty of Levitus data, and the nature of interannual-decadal variations. It is found that the precipitation over the tropical northwestern Pacific is larger in the satellite data (since 1979) than in the Jaeger (1976) data. As a result of the close relationship between SSS and precipitation, the SSS associated with the satellite-derived precipitation is lower than that with the Levitus data.

4 Sensitivity to discrepancies in precipitation observations

Here, we examine the sensitivity of tropical Pacific SST to the discrepancies among different precipitation observations by analyzing results from experiments S1, S2, S3, S4, and S5 (see Table 1 and description in Sect. 2.3). To facilitate the assessment of the significance of this sensitivity, we will also examine the features of experiment S0, in which the effect of $P - E$ is not considered.

Figure 4 shows the difference in SST between S1 and S0. It indicates that the impact of $P - E$ is associated with a general increase in SST in the western and central Pacific, especially in the tropics. In the warm pool, heavy precipitation increases SST by up to 0.6 °C. In the eastern Pacific (e.g., east of 120 °W), SST is generally lower in S1 than in S0. These features occur because $P - E$ changes sign from positive in the western Pacific to negative in the east. For example, as computed from the MSU data, the averaged rainfall rate is 6.7 mm per day over the area of 10 °S–5 °N, 140 °E–170 °E but only 2.7 mm per day over 10 °S–5 °N, 120 °W–90 °W.

Not surprisingly, the SSS pattern of experiment S0 is completely different from that of experiment S1 (figures not shown). Without $P - E$, the model fails to capture both the relatively fresh zone in the Pacific ITCZ and the high SSS zone in the subtropics as shown in Fig. 3b. The climatological SSS field of experiment S0 is characterized by unrealistic, nearly uniform SSS (about 35 psu) over the entire tropical Pacific.

As seen from Fig. 1, over the central-eastern tropical Pacific, the MSU precipitation is much larger than the Jaeger precipitation. To estimate the upper bound for errors in the ocean response to different precipitation climatologies, we analyze the features of ocean response of the experiments using these two precipitation products (S1 and S5). The changes in SST because of the discrepancy between MSU and Jaeger precipitation are shown in Fig. 5a. In the central-eastern tropical Pacific, a noticeable pattern appears in SST difference between S1 and S5. This difference is about 0.2–0.3 °C in the central Pacific but becomes about 1 °C in the eastern Pacific. In general, the higher SST in S1 is associated with the larger precipitation in the MSU product.

Figure 1 also shows that, over the central-eastern tropical Pacific, the MSU precipitation possesses a relatively similar magnitude to the Pathfinder obervation. As a comparison, Fig. 5b shows the difference in SST between S1 (MSU) and S3 (Pathfinder). The SST errors are within 0.2 °C in most of the region. In the

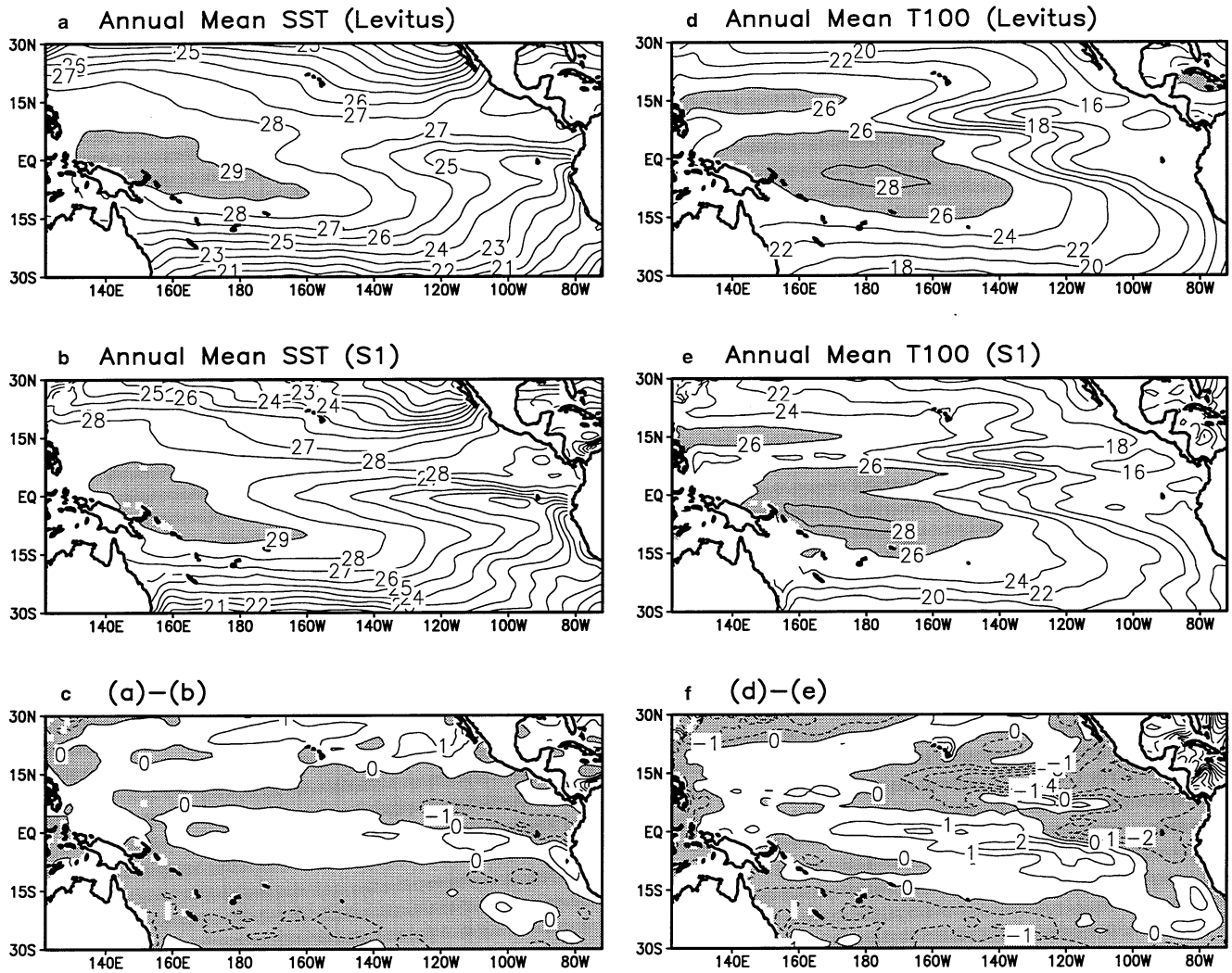

Fig. 2a–f Annaual mean SST (°C) from **a** Levitus data and **b** experiment S1. **c** Shows the observation-simulation SST difference. The corresponding patterns for temperature (°C) at the depth of 100 m are shown in **d**, **e**, and **f**

eastern Pacific, they are much smaller than those shown in Fig. 5a.

It can be seen from the both panels of Fig. 5 that the difference in SST is relatively small in the western tropical Pacific, over which heavy precipitation occurs in all the products. This is due probably to the deeper ocean mixed layer in the western Pacific. In the tropics, the model mixed layer in the western-central Pacific is about twice thicker than that in the eastern ocean.

The pattern of SST rms errors that are calculated among the five experiments (S1, S2, S3, S4, and S5) with different precipitation products is shown in Fig. 6. In the tropics, the errors are mostly smaller than 0.1 °C in the western Pacific. They range between 0.1 °C and 0.2 °C in the central ocean and are larger than 0.3 °C in the eastern pacific. In both hemispheres, large errors appear in the subtropics that are separated by small error zones from the high values in the tropics.

Table 3 list the values of SST rms errors among the various experiments averaged for the Pacific basin (20 °S–20 °N). It shows that the largest difference in SST response occurs among experiment S5 and other experiments, with an average of 0.25 °C (the last column). This magnitude is about 82% of the error that is due to the exclusion of the impact of $P-E$, suggesting the significance of discrepancies between the satellite and non-satellite precipitation products. On the other hand, the smallest rms errors occur between experiments S2 and S3 (0.17 °C) and between S1 and S2 (0.19 °C). Satellite-derived precipitation products (MSU, GPCP, and Pathfinder) are used in these experiments. Overall, the averaged number for all the five experiments is 0.23 °C.

The discrepancies among the various precipitation products are responsible for an averaged rms error of 0.49 psu in the basin-wide SSS. Like SST, SSS varies less significantly within experiments S1, S2 and S3, with

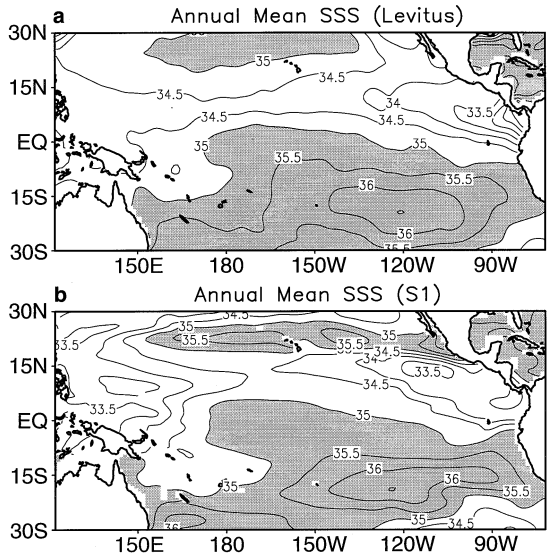

Fig. 3a, b Annual means of sea surface salinity (psu) from **a** Levitus data and **b** experiment S1

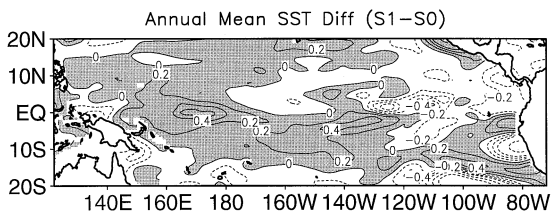

Fig. 4 Difference in annual mean SST between experiments S1 and S0

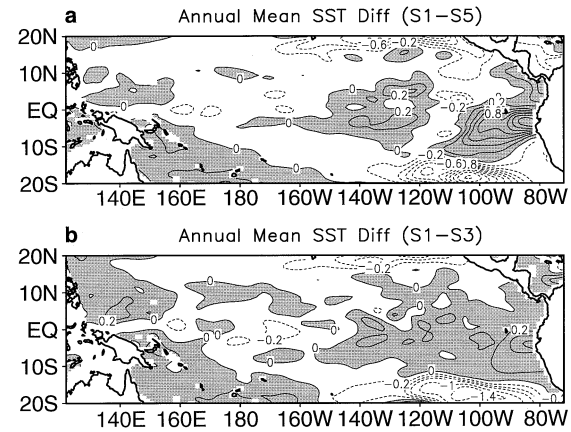

Fig. 5 a Difference in annual mean SST between experiments S1 and S5. **b** Same as **a** but between experiments S1 and S3

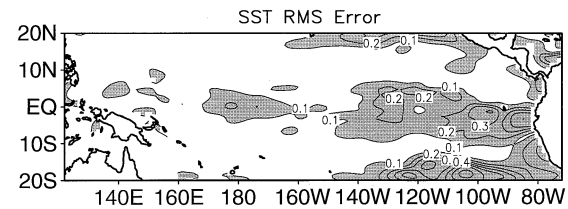

Fig. 6 Root-square-mean errors of SST among experiments S1, S2, S3, S4, and S5

Table 3 Root-mean-square error of SST in °C (20°S–20°N)

	S1	S2	S3	S4	S5
S1	0	0.19	0.24	0.24	0.31
S2		0	0.17	0.22	0.25
S3			0	0.20	0.20
S4				0	0.26
S5					0

an averaged error of 0.31 psu. The largest errors in SSS (0.64 psu, on average) occur between S4 (using CMAP product) and other experiments. The averaged rms error between experiment S5 and other experiments is 0.53 psu.

5 Impact of interannual precipitation anomalies

We have seen that the discrepancies in precipitation products cause a SST error of 0.2–0.3 °C. An interesting question is whether or not this error is significant compared with the change in SST caused by the natural variability of precipitation. To further evaluate the sensitivity of oceanic response to precipitation forcing, we estimate the impact of ENSO related precipitation anomalies on the upper Pacific Ocean. Figure 7a shows that the precipitation over the central-eastern tropical Pacific (10°S–10°N, 160°W–90°W) increased significantly during the winter of 1982–1983 El Niño years. Large enhancement of precipitation is found over a very broad region during January–April 1983, with a maximum enhancement of about 10 mm per day over the central Pacific (Fig. 7b). On the other hand, precipitation reduces moderately over the western equatorial Pacific and most subtropical regions. The precipitation anomalies change not only the total amount of freshwater input to the tropical Pacific but also the gradient of $P-E$ across the ocean.

We estimate the impact of the precipitation anomalies described on the dynamics of upper tropical Pacific by analyzing the results from experiments A1 and A2. The design for these two experiments is identical except that monthly observed MSU precipitation is used in A1 but climatological annual cycle of MSU is applied in A2 (see Table 2). Thus, the difference between the two experiments presumably measures the impact of interannual variations of the MSU precipitation.

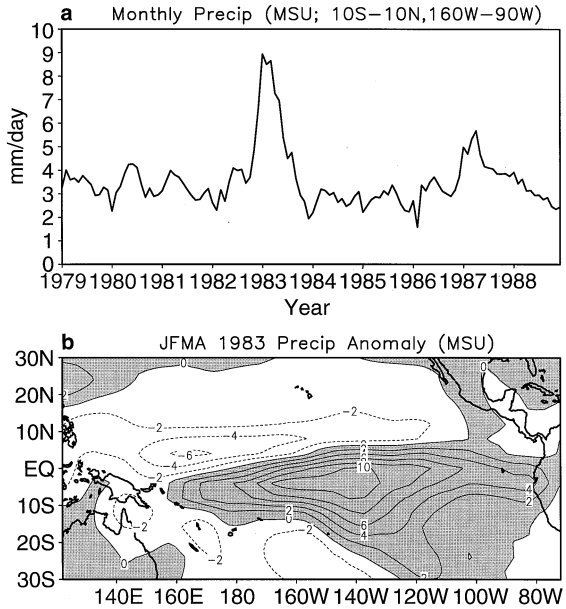

Fig. 7a Monthly MSU precipitation averged over tropical central-eastern Pacific (10 °S–10 °N, 160 °W–90 °W). **b** Precipitation anomalies (mm per day) for January–April of 1983

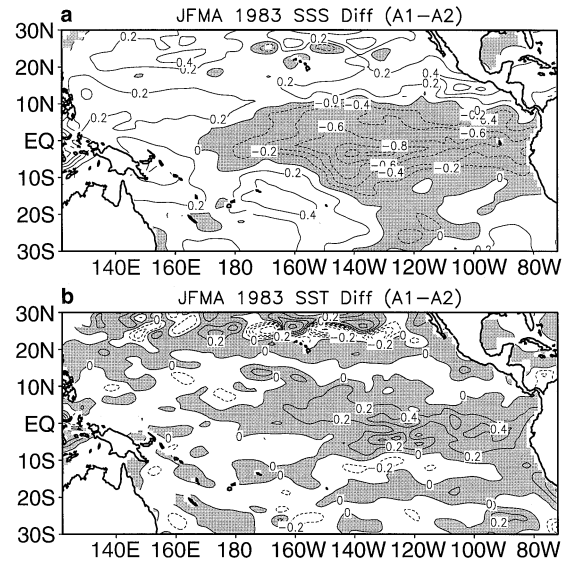

Fig. 8a, b Differences in **a** SSS and **b** SST between experiments A1 and A2

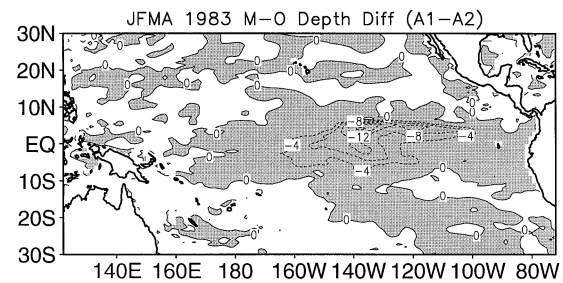

Fig. 9 Difference in Monin-Obukhov depth (in m) between experiments A1 and A2

Figure 8 shows the response of SSS and SST to the precipitation anomalies illustrated in Fig. 7. Associated with the enhanced precipitation, SSS decreases dramatically in the central-eastern tropical Pacific (Fig. 8a). Near the maximum center of precipitation anomalies, the seasonal mean SSS drops by 1 psu. At the same time, SSS increases in the regions of negative precipitation anomalies.

Figure 8b indicates that SST increases in the central-eastern tropical Pacific. This demonstrates again that freshwater input raises SST. The enhanced precipitation shown in Fig. 7b increases SST by 0.2–0.4 °C in a broad region. In some locations, the value is even as high as 0.6 °C. The magnitude of this gain in SST caused by the enhanced precipitation is about 10–15% of the total SST increase observed during the winter, which is due largely to the effect of wind stress. Only small SST changes occur outside the region of highly positive precipitation anomalies, with an exception in the northern subtropics.

The addition of freshwater to the ocean results in a downward surface buoyancy flux. This suppresses vertical mixing. In regions of net positive downward buoyancy flux, the mixed layer depth is largely determined by the Monin-Obukhov depth, the ratio of wind generation of turbulent kinetic energy to the buoyancy flux. Increasing the buoyancy flux decreases the Monin-Obukhov depth, and consequently decreases the surface mixed layer depth. Figure 9 shows the change in Monin-Obukhov depth during January-April of 1983 winter between experiments A1 and A2. The dominant feature of the figure is the decrease in the Monin-Obukhov depth in the central-eastern Pacific.

While to first order, the change in the Monin-Obukhov depth should not have a direct impact on the equilibrium SST. Virtually all the relevant higher order terms (horizontal advection, vertical diffusion, and others) will lead to higher surface temperatures with shallower mixed layers. The results shown in Figs. 8 and 9 bear this out: while the Monin-Obukhov depth changes by 20–30% in the eastern tropical Pacific, the net surface heat flux in this region changes by only 2–5%.

Figure 10a, which shows the pattern of difference in sea surface height, indicates an apparent rise in sea level associated with the enhancement of precipitation. The rise in sea level in the central-eastern tropics decreases the zonal pressure gradient. Figure 10b clearly shows an intensification of the westward surface current in the tropical Pacific. The surface current is enhanced by the shallowing mixed layer and the reduced pressure gradient. Corresponding to the precipitation anomaly, stronger signal of the current occurs in the Southern Hemisphere. To some extent, the result shown in Fig. 10b is similar to that obtained by Reason (1992, see

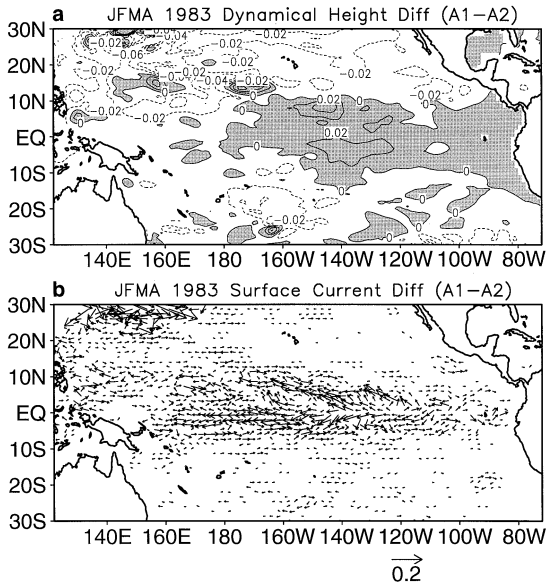

Fig. 10a, b Differences in **a** sea surface height (in m) and **b** surface current (in ms^{-1}) between experiments A1 and A2

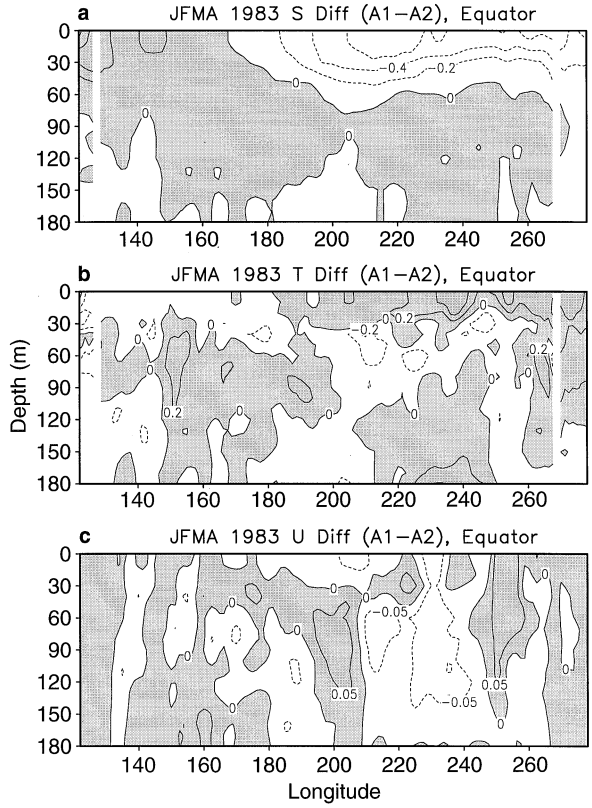

Fig. 11a–c Vertical profiles of differences in salinity, temperature, and zonal current (in ms^{-1}) between experiments A1 and A2 for January–April 1983

his Fig. 9), who performed two experiments using the Geophysical Fluid Dynamics Laboratory ocean model (Cox 1984) to understand the influence of El Niño and La Niña type precipitation forcing on ocean salinity and surface current.

We examine now the changes in the vertical structure of equatorial upper ocean because of the interannual variability of precipitation. Figure 11 shows the differences, between experiments A1 and A2, in salinity, zonal current, and temperature for January–April 1983. The increase in precipitation during the El Niño period causes a significant, broad-scale drop in salinity within the upper 60 m (Fig. 11a). However, there is no signal under those upper layers. The warming in the freshening water of the central-eastern Pacific is evident, but it is mainly limited to the upper 30 m, beneath which the ocean becomes cooler. In the western Pacific, the reduced precipitation during the El Niño period decreases slightly the temperature of the surface layer and increases the temperature underneath.

The change in the vertical profile of temperature reflects the importance of vertical mixing in the upper layers. In the central-eastern Pacific, the fresher and warmer surface layer stabilizes the upper ocean and suppresses vertical mixing. As a result, the temperature under the warming layer tends to be cooler. The change in temperature structure in the west Pacific seems reversed because of the decrease in precipitation. The change in temperature shown in Fig. 11b is also associated with a flattening of the thermocline in the eastern Pacific, as found from the change in the 20 °C isotherm.

It has been shown in Fig. 10b that the enhanced precipitation over the central-eastern Pacific is accompanied by intensification of surface current. Figure 11c indicates that the returning eastward current under the surface layer also becomes slightly stronger in the western-central Pacific. The stronger eastward current leads to large subsurface mass transport from the warm west to the cool east, helping to maintain the warming in the central-eastern Pacific. As an evidence, the subsurface cooling in the central Pacific shown in Fig. 11b. becomes weaker by October–November 1983 when precipitation forcing subsides. This current-temperature relationship is demonstrated more clearly in Fig. 14, which will be discussed soon.

It is also instructive to examine the response of upper ocean to the precipitation anomalies during La Niña years. During January–April 1985, below normal precipitation occurred over the tropical Pacific especially over the central-eastern ocean (Fig. 12a). This reduction in precipitation is associated with an increase in ocean salinity and thus buoyancy flux. Figure 12b shows that the Monin-Obukhov depth increases significantly, indicating that the upper ocean becomes less stable. The decreased stability leads to stronger vertical mixing in the upper ocean, which causes a decrease in SST (Fig. 12c). Therefore, in contrast to the excessive precipitation during El Niño years that increases SST as shown above, the deficient precipitation during La Niña years decreases the values of SST. The results

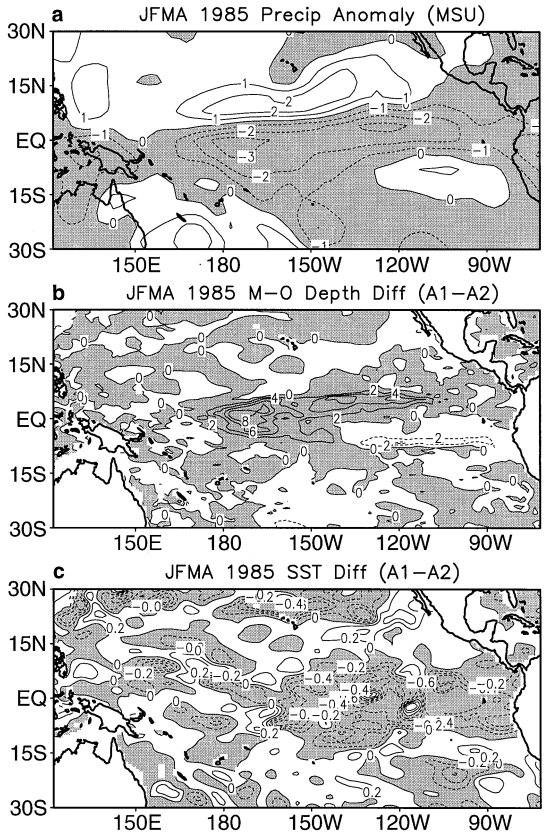

Fig. 12 a MSU precipitation anomalies for January–April of 1985. Also shown in the figure are the January–April 1985 difference (A1 minus A2) patterns for **b** Monin-Obukhov depth and **c** SST

shown in Figs. 8 and 12 indicate that the relationship between precipitation anomalies and SST variability is nonlinear. Compared to freshwater input, the deficiency in precipitation affects ocean temperature more effectively because of the direct influence of the intensified vertical mixing that brings up cool water from below. It should be pointed out that an examination of the winter of 1985–86 yields similar results to those shown in Fig. 12.

6 Further experiments

It is postulated that the features of oceanic response shown in the two earlier sections will become more eminent when precipitation forcing is stronger. Because of the spatial difference in upper ocean structure such as the mixed layer and thermocline, it is also assumed that a forcing will cause different response when it is placed in different locations. To confirm these features, we carry out further experiments with specified forcings. In particular, we perform four additional experiments that are referred to as CLI (climatology), WPF (western Pacific forcing), CPF (central Pacific forcing), and EPF (eastern Pacific forcing), respectively. The designs of these experiments is similar to those shown in Table 1 except that different precipitation forcing is used and the model is run for two years. The forcing used in CLI is the time-independent annual mean of MSU precipitation. In experiments WPF, CPF, and EPF, the precipitation forcing is the same as that used in CLI except that an identical forcing of 16 mm per day is superimposed over the western, central, and eastern Pacific, respectively (see the boxes in Fig. 13).

Figure 13 shows the patterns of difference in the temperature and salinity averaged within the top 50 m between each "anomaly" experiment (WPF, CPF, or EPF) and CLI. The pattern in each panel can be viewed as the temperature or salinity responses to the specified precipitation forcing that is confined in the box. Thus, the figure depicts how the temperature and salinity respond differently to an identical precipitation forcing that is placed over different locations.

The figure shows that when an identical precipitation forcing is placed in different locations, the response of upper ocean is different. When freshwater is added into the equatorial regions, divergent surface current transports surface salinity anomaly off the equator. This is noticeable in experiments CPF and EPF, but not in WPF because of the effect of western boundary. Interesting features also appear in the changes of temperature. Figures 13d–f show that, although the upper ocean generally becomes warmer regardless of the location of the forcing, obvious signals occur in a different region in each experiment. When precipitation anomaly is over the western Pacific, warming occurs within and to the east of the forcing. However, when precipitation anomaly is over the central ocean, warming appears within the forcing region. Finally, when precipitation anomaly is placed over the eastern Pacific, temperature increases within and to the west of the forcing. Figure 13 also indicates that the response of upper ocean is strongest when the precipitation forcing is over the eastern Pacific because of the shallowest thermocline.

To gain a better understanding of the features about upper ocean response to the specified freshwater forcing, we show in Fig. 14 changes in vertical profiles of salinity, surface current, and temperature. In WPF (Fig. 14a–c), the salinity anomaly is confined to the upper 50 m. Along the equator, a shallowing Monin-Obukhov depth allows an eastward anomaly of surface current of 0.1–0.15 ms^{-1} to the east of the forcing. The concentrating salinity anomaly in the western Pacific increases the pressure gradient across the basin, reducing the zonal current. The warming in the cold tongue appears to be a result of deepening of the thermocline across the basin. In CPF, although the salinity anomaly is advected away from the equator by the divergent surface current, a freshening amount of more than 0.12 psu is seen to a depth of 100 m at the equator. The equatorial current increases, bringing warm water from

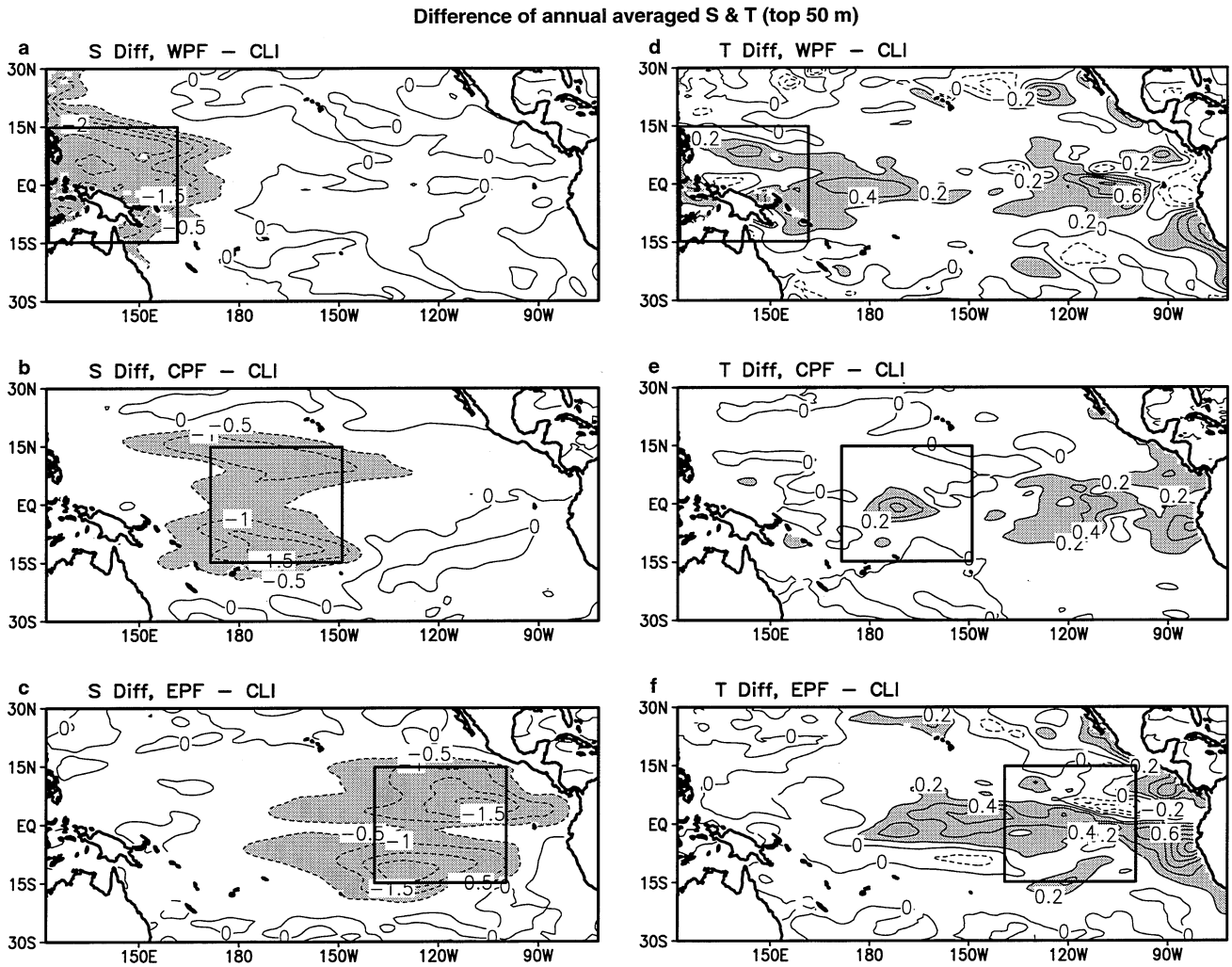

Fig. 13 **a** Difference in the annual salinity, averaged within top 50 m, between experiments WPF nd CLI. **b** Same as **a** but between CPF and CLI; **c** same as **a** but between EPF and CLI. The box in each panel shows the location of time-independent precipitation forcing of 16 mm per day. The corresponding patterns for temperature are shown in **d**, **e**, and **f**

the western Pacific to the base of the cold tongue. The ocean response in experiment EPF is similar to that in CPF but different from that in WPF. The salinity decreases throughout the upper 60 m. The increased stability and shallower Monin-Obukhov depth permit the net surface heating to increase the SST in the cold tongue. The westward advection by the surface current carries the SST signal out to the dateline. In this experiment, the under current is also accelerated by more than 0.1 ms^{-1}.

The trapping of the salinity to the upper equatorial Pacific in the WPF experiment is consistent with the schematic view of the formation of the barrier layer presented in Vialard and Delecluse (1998). The salinity anomaly added to the west of the warm pool salinity front remains trapped to the surface and confined behind the front. When the forcing is introduced to the east of the front (in CPF), the salinity anomaly is seen to be advected downward and westward, under the salinity front. In addition, it is advected poleward and westward.

It can be seen that the ocean response in experiments CPF and EPF is similar to the response to the enhanced precipitation during ENSO as shown in Figs. 8–11. In all experiments, the SST response consists of a local response because of shallowing Monin-Obukhov depth and an eastern Pacific response because of the advection of the Equatorial Undercurrent. Corresponding changes also occur in the basin-wide thermocline.

7 Summary and discussion

In this study, we have performed a series of experiments using an ocean model to study the sensitivity of tropical Pacific Ocean to variations in precipitation induced

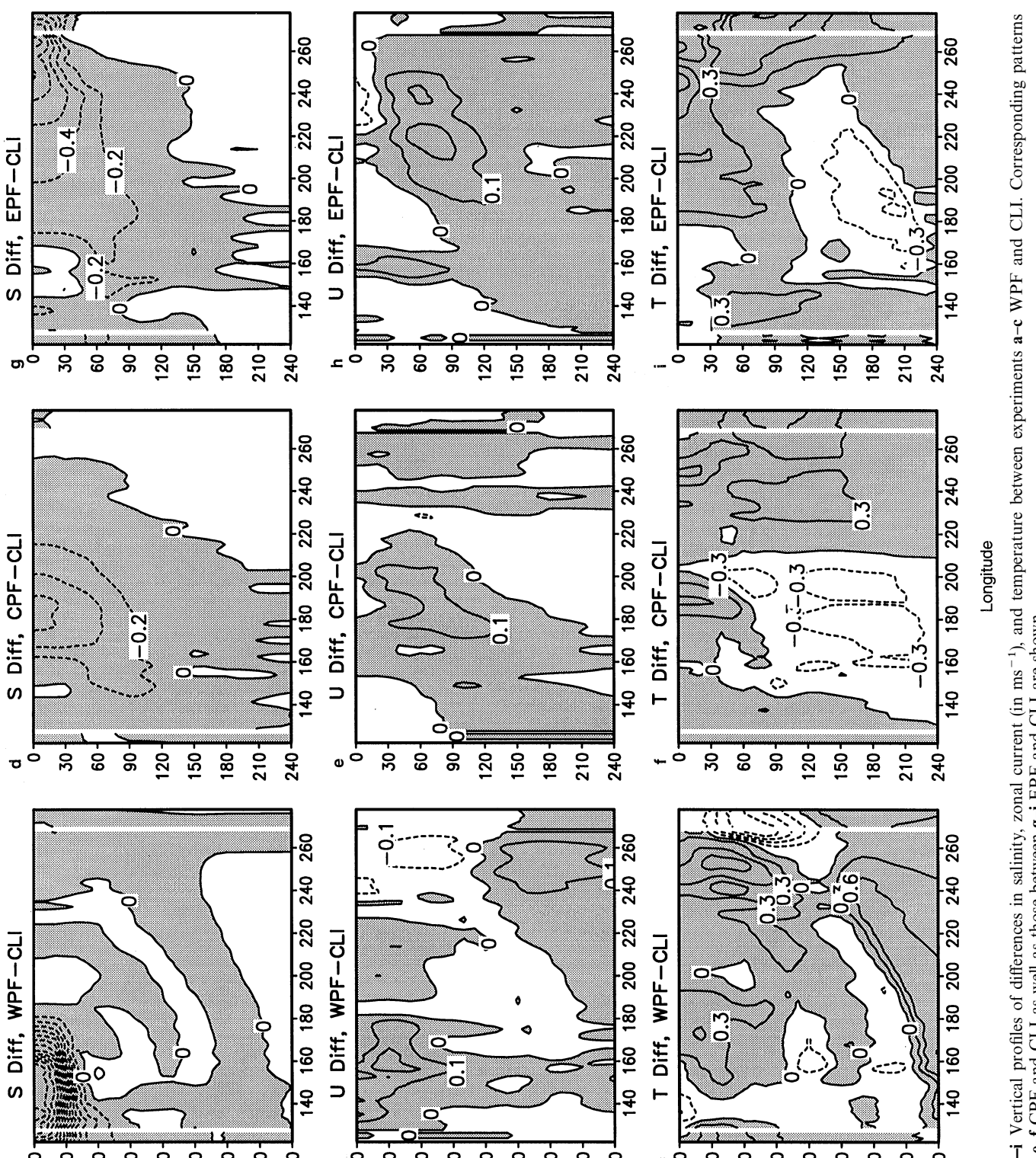

Fig. 14a–i Vertical profiles of differences in salinity, zonal current (in ms^{-1}), and temperature between experiments **a–c** WPF and CLI. Corresponding patterns between **e–f** CPF and CLI as well as those between **g–i** EPF and CLI are shown

freshwater fluxes. The model used is a quasi-isopycnal model, covering the Pacific from 40 °S to 40 °N. The surface forcing is constructed from observed wind stress, evaporation, precipitation, and SST fields. The heat flux is produced with an iterative technique so as to maintain the model close to the observed climatology, but with only weak damping to that climatology. Climatological estimates of evaporation are combined with various estimates of precipitation to determine the net surface freshwater flux.

Results indicate that increased freshwater input decreases salinity, but increases temperatures in the upper ocean. Using the freshwater flux estimated from the MSU leads to a warming of up to 0.6 °C in the western Pacific over a case with zero net freshwater flux. SST is sensitive to the discrepancies among different precipitation observations, with root-mean-square difference in SST on the order of 0.2–0.3 °C. The change in SST is more pronounced in the eastern Pacific, with difference of over 1 °C found among the various precipitation products. Interannual variation in precipitation during El Niño events leads to increased warming. During the winter of 1982–83, freshwater flux accounts for about 0.4 °C (approximately 10–15% of the maximum warming) of the surface warming in the central-eastern Pacific. Thus, the error of SST caused by the discrepancies in precipitation products is more than half of the SST anomaly produces by the interannual variability of observed precipitation.

Further experiments, in which freshwater flux anomalies are imposed in the western, central, and eastern Pacific, show that the influence of net freshwater flux is also spatially dependent. The imposition of freshwater flux in the far western Pacific leads to a trapping of salinity anomaly to the surface layers near the equator. An identical flux imposed in the central Pacific leads to deeper and off-equatorial salinity anomalies. The contrast between these two simulations is consistent with other simulations of the western Pacific barrier layer formation.

Precipitation increases the temperature of upper ocean through both local buoyancy effect and remote advective effect. Freshwater input reduces ocean salinity and buoyancy flux. As a result of weakened vertical mixing, temperature increases. The warming of the upper ocean further reduces buoyancy flux and stabilizes the ocean. Such a positive interaction favors a further increase in SST. The enhanced precipitation anomaly over the central-eastern Pacific intensifies surface current and the Equatorial Undercurrent. Accordingly, the thermocline flattens slightly and more warm water is transported from the west to the east. This advective effect becomes more evident when strong atmospheric hydrologic forcing is placed over the eastern Pacific.

There is no doubt that for seasonal-to-interannual time scales wind stress is of primary importance for the dynamics of the world's oceans. However, the effect of freshwater flux cannot be neglected for realistic ocean simulations. Because the various precipitation products cause different responses of the upper ocean, choosing an appropriate precipitation product as atmospheric hydrologic forcing is important in ocean modeling. This issue may be of special importance because there are currently many precipitation products and the number of precipitation products will increase in the future.

In this study, only seasonal and annual averaged patterns have been analyzed. Because all of the surface forcing fields used are on monthly mean time scales, we are unable to analyze the high frequency features of ocean response caused by submonthly forcing. Intraseasonal variability is a prominent feature of the tropical atmosphere. It is expected that an inclusion of this feature in precipitation forcing field will reveal more detailed features of ocean response of shorter time scales.

Another important issue that has not been addressed by this study is the physical significance of the SST anomalies caused by the precipitation induced freshwater flux. For example, to what extent will the atmosphere respond to these SST anomalies? To answer this question, it is desirable to conduct several experiments using an atmospheric GCM. In these experiments, the atmospheric model is forced by different SST anomalies that have been generated by the ocean model from this study. The significance of the SST's impact can be assessed by analyzing the response of the atmosphere.

Acknowledgements We thank Drs. Bohua Huang, Roger Lukas, Michele Rienecker, Max Suarez, and Zuojun Yu for many helpful discussions. We especially thank Dr. Zuojun Yu for her help in model improvement and useful comments to improve the quality of this paper. Thanks are also to Dr. Bohua Huang for providing the FSU wind stress data. Drs. George Huffman and Pingping Xie for some precipitation data, and Dr. Liping Wang for the Levitus data. Helpful comments from the two anonymous reviewers are appreciated. This study was supported by the NASA Tropical Rainfall Measuring Mission (TRMM) Project and the Global Modeling and Analysis Program, both of the Earth Enterprise, NASA Headquarters.

References

Anderson SP, Weller RA, Lukas RB (1996) Surface buoyancy forcing and the mixed Layer of the Western Pacific Warm Pool: Observations and ID model results. J Clim 9: 3056–3085

Ando K, McPhaden MJ (1997) Variability of surface layer hydrography in the tropical Pacific Ocean. J Geophys Res 102: 23 063–23 078

Carton JA (1991) Effect of seasonal surface freshwater flux on sea surface temperature in the tropical Atlantic Ocean. J Geophys Res 96: 12 593–12 598

Cooper NS (1988) The effect of salinity on tropical ocean models. J Phys Oceanogr 18: 697–707

Cox MD (1984) A primitive equation, 3-dimensional model of the ocean. GFDL Ocean Group Tech Rep 1, GFDL/Princeton University, USA

Cronin MF, McPhaden MJ (1988) Comparison of the upper ocean heat and freshwater balances in the western Pacific warm-fresh pool. AMS Preprint, Ninth Conf on Interaction of the Sea and Atmosphere, 11–16 January 1998, Phoenix, Arizona, USA, 157–158

Gill AE (1982) Atmosphere-ocean dynamics. Academic Press, London, UK, pp 662

Godfrey JS, Lindstrom EJ (1989) The heat budget of the equatorial western Pacific surface mixed layer. J Geophys Res 94(C6): 8007–8017

Haney RL (1971) Surface thermal boundary condition for ocean circulation models. J Phys Oceanogr 1 : 214–248

Hellerman S, Rosaenstein M (1983) Normal monthly wind stress over the world ocean with error estimates. J Phys Oceanogr 13 : 1093–1104

Hough SS (1897) On the application of harmonic analysis to the dynamical theory of the tides. Part I. On Laplace's 'oscillation of the first species', and on the dynamics of ocean currents. Philos Trans R Soc London Ser A 189 : 201–257

Huang RX (1993) Real freshwater flux as a natural boundary condition for salinity balance and thermohaline circulation forced by evaporation and precipitation. J Phys Oceanogr 23 : 2428–2446

Huffman GJ, Adler RF, Arkin P, Chang A, Ferraro R, Gruber A, Janowiak J, McNab A, Rudolf B, Schneider U (1997) The Global Precipitation Climatology Project (GPCP) combined precipitation dataset. Bull Am Meteorol Soc 78 : 5–20

Jaeger L (1976) Monatskarten des Niedershlads für die ganz Erde. Ber Dtsch Wetterdienste 139, 33pp plus plates

Lau K-M, Sud C, Kim J-M (1996) Intercomparison of hydrologic processes in AMIP GCMs. Bull Am Meteorol Soc 77 : 2209–2227

Levitus S (1982) Climatological Atlas of the World Ocean. NOAA Prof Pap US Government Printing Office, Washington, DC 20402 73pp

Li X, Sui C, Adamec D, Lau K-M (1998) Impacts of precipitation in the upper ocean in the western Pacific warm pool during TOGA COARE. J Geophys Res 103 : 5347–5359

Lukas R, Lindstrom E (1991) The mixed layer of the western equatorial Pacific Ocean. J Geophys Res 96 (suppl) : 3343–3357

Miller JR (1976) The salinity effect in a mixed-layer ocean model. J Phys Oceanogr 6 : 29–35

Murtugudde R, Busalacchi AJ (1998) Salinity effects in a tropical ocean model. J Geophys Res 103 : 3283–3300

Niiler PP, Kraus EB (1977) One-dimensional models of the upper ocean. In: Kraus EB (ed) Modelling and prediction of the upper layers of the ocean. Pergamon, Oxford, pp 143–172

Pacanowski R, Philander SGH (1981) Parameterization of vertical mixing in numerical models of tropical oceans. J. Phys Oceanogr 11 : 1443–1451

Price JF (1979) Observations of a rain-formed mixed layer. J. Phys Oceanogr 9 : 643–649

Reason CJC (1992) On the effect of ENSO precipitation anomalies in a global ocean GCM. Clim Dyn 8 : 39–47

Reynolds RW, Smith TM (1994) Improved global sea surface temperature analyses using optimum interpolation. J Clim 7 : 929–948

Schopf PS (1985) Modeling tropical sea surface temperature: implications of various atmospheric responses. In: Nihoul JCJ (ed) Coupled ocean-atmosphere models. Elsevier, Amsterdam, pp 727–734

Schopf PS, Loughe A (1995) A reduced gravity isopycnal ocean model: Hindcasts of El Niño. Mon Weather Rev 123 : 2839–2863

Shapiro R (1970) Smoothing, filtering and boundary effects. Rev Geophys Space Phys 8 : 359–387

Spencer RW (1993) Global oceanic precipitation from the MSU during 1979–1991 and comparisons to other climatologies. J Clim 6 : 1301–1326

Vialard J, Delecluse P (1998) An OGCM study for the TOGA decade. Part II: Barrier layer formation and variability. Tech Rep 4, Institute Pierre Simon Laplace, Paris, France

Webster PJ, Lukas R (1992) TOGA COARE: The Coupled Ocean-Atmosphere Response Experiment. Bull Am Meteorol Soc 73 : 1377–1416

Weller RA, Anderson SP (1996) Surface meteorology and air–sea fluxes in the western equatorial Pacific warm pool during the TOGA Coupled Ocean–Atmosphere Response Experiment. J Clim 9 : 1959–1990

Xie P, Arkin PA (1996) Analyses of global monthly precipitation using gauge observations, satellite estimates and numerical model predictions. J Clim 9 : 840·–858

You Y (1995) Salinity variability and its role in the barrier layer formation during TOGA COARE. J Phys Oceanogr 25: 2778–2807

Yu Z, Schopf PS (1997) Vertical eddy mixing in the tropical upper ocean: Its influence on zonal currents. J Phys Oceanogr 27 : 1447–1458

Yu Z, Schopf PS, McCreary JP (1997) On the annual cycle of upper-ocean circulation in the eastern equatorial pacific. J Phys Oceanogr 27 : 309–324